Studies of the Radiation Environment on the Martian Surface Using the Geant4 Toolkit

Authors: Chen, Jun-Liang, Yun, Su-Jun, Dong, Tie-Kuang, Ren, Zhong-Zhou, Zhang, Xiao-Ping, Dong, Tie-Kuang, Ren, Zhong-Zhou

Date: 2021-12-31T14:48:57+00:00

Abstract

The radiation environment on the surface of Mars is a potential threat for future manned exploration missions to this planet. In this study, a simple geometrical model was built for simulating the radiation environment on the Mars surface caused by galactic cosmic rays (GCRs); the model was built and studied using the Geant4 toolkit. The simulation results were compared with the data reported by a radiation assessment detector (RAD).

Full Text

Preamble

Studies of the radiation environment on the Mars surface using the Geant4 toolkit

Jun-Liang Chen[1], Su-Jun Yun[2], Tie-Kuang Dong[3],†, Zhong-Zhou Ren[4],‡, and Xiao-Ping Zhang[5]

[1]Key Laboratory of Modern Acoustics and Department of Physics, Nanjing University, Nanjing 210093, China
[2]School of Electronic Engineering, Nanjing XiaoZhuang University, Hongjing Road, Nanjing 211171, China
[3]Key Laboratory of Dark Matter and Space Astronomy, Purple Mountain Observatory, CAS, 2 West Beijing Road, Nanjing 210008, China
[4]School of Physics Science and Engineering, Tongji University, Siping Road 1239, Shanghai 200092, China
[5]State Key Laboratory of Lunar and Planetary Sciences, Macau University of Science and Technology, Macao 999078, China

The radiation environment on the surface of Mars poses a potential threat to future manned exploration missions to the planet. In this study, we constructed

a simple geometrical model to simulate the radiation environment on the Martian surface caused by galactic cosmic rays (GCRs) using the Geant4 toolkit. The simulation results were compared with data reported by the Radiation Assessment Detector (RAD).

The simulated spectra of neutrons, photons, protons, α particles, and particle groups Z = 3–5, Z = 6–8, Z = 9–13, and Z = 14–24 showed reasonable agreement with RAD data. However, for deuterons, tritons, and ^{3}He, the simulations yielded much smaller values than the corresponding RAD measurements. Additionally, particle spectra within a 90° zenith angle were obtained. Based on these spectra, we calculated the radiation dose that would be received by an average human body on Mars. The dose distribution throughout the human body was not uniform. The brain received the highest absorbed and equivalent doses among all organs, reaching 62.0$\pm$1.7$mGy/yand$234.1$\pm$8.0 mSv/y, respectively. The average absorbed and equivalent doses for the entire body were approximately 44 mGy/y and 153 mSv/y, respectively. Further analysis revealed that most of the radiation dose was attributable to α particles, protons, and heavy ions. We subsequently investigated the shielding effect of Martian soil against radiation. The body dose decreased significantly with increasing soil depth. At a depth of 1.5 m, the effective dose for the entire body was 17.9$\pm$2.4$mSv/y, lowerthantheoccupationalexposuredoselimit.Atadepthof3m,theeffectivedosetothebodywa$ mSv/y, still higher than the accepted public dose limit.

Keywords: Galactic cosmic rays, Radiation environment of Mars, Absorbed dose, Equivalent dose, Geant4

Introduction

Space exploration has developed rapidly, with significant progress achieved in recent decades. Mars has become a hotspot for deep-space exploration missions, with programs designed to understand its evolution and determine whether life exists on the planet [1]. Manned missions to Mars are also on schedule [2]. A critical factor that must be considered for manned space exploration is space radiation, which originates from galactic cosmic rays (GCRs) and solar particle events (SPEs) [3–5].

In space, energetic particles can penetrate spacecraft and harm both instruments and astronauts [6]. Radiation-related health risks constitute a serious challenge for long-term manned space exploration missions [7,8]. GCRs are mainly composed of charged nuclei, such as protons, α particles, and heavier nuclei with a broad energy range from sub-MeV to hundreds of TeV [9,10]. SPEs consist primarily of protons and α particles with relatively lower energies compared to GCRs. Due to Mars' thin atmospheric layer and lack of a global magnetic field [11], the radiation intensity on its surface is much higher than on Earth. Understanding the radiation environment on Mars and the likely dose to astronauts is crucial for planning future manned missions [11,12], as it enables accurate assessment of health risks and provides a reference for designing radiation protection

gear [13,14].

The radiation environment on Mars is complex and defined by several factors. The shielding effect of the Martian atmosphere is much weaker than Earth' s. Consequently, energetic particles in GCRs and SPEs can penetrate the Martian atmosphere and reach the planet' s surface. Due to the irregularity and infrequency of SPEs, only GCRs were considered in this study. Interactions between GCRs and atmospheric molecules generate numerous secondary particles, which further interact with the atmosphere, resulting in a complex radiation spectrum on the Martian surface. Albedo particles produced on the planet' s surface also contribute to the radiation environment. These three main components of the surface radiation environment were considered in our study. The Curiosity rover has conducted long-term scientific exploration on Mars since its successful landing in 2012, and its onboard Radiation Assessment Detector (RAD) has been collecting radiation-related information, including particle spectra and absorbed dose rates [15].

Studies have shown that long-term exposure to space radiation can harm humans [2]. Radiation can directly and indirectly affect DNA molecules, causing cell death or mutation and increasing cancer risk [16–18] and other diseases. NASA has categorized space radiation health risks into four groups: 1) degenerative tissue effects, 2) carcinogenesis, 3) acute and late central nervous system (CNS) effects, and 4) radiation-related syndromes [19]. Accurate calculation of radiation doses received by astronauts is necessary for assessing these health risks. However, directly calculating particle spectra on the Martian surface and associated radiation doses is difficult. Monte Carlo simulations can address this problem, and several transport codes have been used to study the radiation environment in space and on Mars, including HZETRN [20,21], HETC-HEDS [22], FLUKA [23], PHITS [24], MCNP6 [25,26], and Geant4 [27–30].

Most previous studies have focused primarily on simulating the surface radiation environment. Our work addresses two aspects of this research area. First, we used the G4QMD model to handle inelastic scattering of GCRs in the Martian atmosphere and soil to obtain particle spectra on the surface. Then, based on these simulated spectra, we calculated the radiation dose received by a typical human body. To our knowledge, this is the first study attempting to estimate radiation dosage to individual organs of a typical human on the Martian surface. These results and conclusions can inform planning for future manned Mars exploration missions.

II. The Radiation Environment on Mars

A. Model Setup

To reduce simulation time, we built a simple geometrical model consisting of a cylinder (radius: 1 km) to represent the Martian environment. The cylinder was divided into 12 layers to represent Martian regolith and atmosphere. The bottom layer corresponded to Martian regolith (thickness: 3 m; density: 1.7

g/cm^3) [21]. The second layer was 4 m thick, representing surface atmospheric conditions. Layers three through twelve were each 1 m thick, with column densities of 11.820, 5.915, 2.624, 1.069, 0.395, 0.131, 0.035, 0.009, 0.003, and 0.001 g/cm^2, respectively. The overall column density of these layers was approximately 22 g/cm^2 [21,31,32], representing the Martian atmosphere. The detector was a cylinder (radius: 1 km; thickness: 3 mm) positioned 1 m above the soil to detect and register the Martian radiation environment. Soil and atmospheric components (Table 1) were derived from Ref. [21]. Primary GCRs were isotropically incident from the top of the geometrical structure, and particle information—including type, kinetic energy, and angle of incidence—was recorded upon passing through the detector.

Table 1. Modeled soil and atmosphere components of Mars [21].

Component	Composition
Martian atmosphere	CO_2 (95.7%), N (2.7%), Ar (1.6%)
Martian soil	SiO_2 (51.2%), Fe_2O_3 (9.3%), H_2O (7.4%), $Al_2CaK_2MgNa_2O_7$ (32.1%)

Simulations were performed using Geant4-10.5.1, a track-structure code developed at CERN for simulating particle passage through matter [29,30]. Geant4 provides numerous user-selectable models for specific applications and has been widely used in high-energy physics, medical physics, and radiobiology. The physical parameters used for simulating GCR interactions with the Martian medium are listed in Table 2. The Emstandard_{opt3} physics list described electromagnetic interactions of photons, leptons, hadrons, and ions in the 1 keV–10 PeV range [33]. The G4HadronPhysicsQGSP_{BIC}_{HP} physics list [34] described inelastic scattering of nucleons and mesons with nuclei in the 0 eV–100 TeV range. This list uses the quark-gluon string model (QGS) for high-energy hadronic interactions (12 GeV–100 TeV), the binary cascade model (BIC) for intermediate-energy nucleon-nucleus interactions, and high-precision neutron models (HPs) for neutron-nucleus interactions below 20 MeV. For inelastic nucleus-nucleus interactions, we used the G4QMD model validated in our previous work [35], where all nucleons are considered participant particles treated as Gaussian wave packets, with particle motion equations derived from the time-dependent variation principle [36]. Detailed descriptions appear in the Geant4 Physics Reference Manual [36].

Table 2. Physics models used in simulations.

Interaction type	Model
Electromagnetic	Emstandard_{opt3}
Hadronic inelastic	G4HadronPhysicQGSP_{BIC}_{HP}
Hadronic inelastic for ions	G4IonQMDPhysics

Only GCRs were considered as contributors to the Martian radiation environment. GCRs mainly consist of protons, α particles, and heavy ions. Although heavy particles constitute a very small fraction, they are important for radiation protection due to their high relative biological effectiveness (RBE). Our simulations considered particles with atomic numbers Z = 1–26. Energy spectra were calculated using the GCR model developed by Matthiä et al. [10], which uses a single parameter W to describe solar activity modulation [10]. Figure 1 shows a portion of the primary GCR spectra used in the simulation. The modulation parameter W was calculated according to the Oulu neutron monitor count rate (from http://cosmicrays.oulu.fi/) during August 2012 to January 2013, with an average value W = 56 used in this work.

B. Results

When GCRs pass through a planetary atmosphere, many neutrons and photons are induced through interactions with atmospheric molecules. Figure 2 shows the simulated neutron and photon spectra on the Martian surface alongside experimental data [21,37]. Simulation results for neutrons were slightly higher than experimental data below 100 MeV/n, while photon results agreed well with RAD data. Average relative deviations were 60.8% for neutrons and 56.0% for photons.

Simulated charged particle spectra for zenith angles smaller than 30° are plotted in Figures 3 and 4. Heavy particles were divided into groups for comparison with RAD data [15]. The simulated spectra of protons, α particles, and groups Z = 6–9, Z = 9–13, and Z = 14–24 were consistent with RAD data, with average relative deviations of 27.7%, 37.9%, 40.9%, 60.7%, and 40.1%, respectively. For groups Z = 3–5 and Z > 24, simulation results were slightly lower than measured data. However, simulated spectra of deuterons, tritons, and ^{3}He were much lower than RAD data, with an average relative deviation of approximately 90%. These pure secondary particles are generated in reactions between primary GCRs and atmospheric molecules, and the discrepancy likely arises from lower generation cross-sections. Previous work showed that G4QMD model cross-sections for light fragments were lower than experimental data [35].

Heavy charged particles from the entire upper hemisphere were also recorded. Simulated spectra for zenith angles smaller than 90° are plotted in Figure 5. For light particles, the flux averaged over 90° was close to that for angles below 30°, while for heavy particles, the flux below 90° was slightly smaller than that below 30°. Spectra of electrons, muons, and pions were also calculated due to their significant contributions to absorbed dose (Figure 6).

III. Radiation Dose Received by a Typical Human Body

Accurate dose estimation for astronauts is essential for successful manned deep-space exploration. Additionally, with widespread nuclear technology use in material and medical physics [38–46], calculating radiation doses to typical humans

in corresponding environments is important. Based on our simulation results, we calculated the radiation dose that would be received by a human body on Mars.

A. Model Setup

The geometrical simulation model is shown in Figure 7. The human phantom model [48] was taken from the Geant4 advanced example "human phantom" and placed on the Martian surface. A cubical regolith block ($10\$\times10\times6m^{\{3\})withdensity1.7g/cm}\{3\}\$$ was constructed. The simulated particle spectra within 90° zenith angle (from Figures 5–6) were used as primary particles projected onto the surface from the top of the model. For each simulation step, energy deposited by different particles into various organs was recorded. After simulation, total deposited energy, absorbed dose, and equivalent dose delivered by different particles to different organs were calculated. The total sampling number for each primary particle was set to 5 million. Each scenario was repeated six times, with uncertainties representing one standard deviation from the mean.

According to the International Commission on Radiological Protection (ICRP) [47], the equivalent dose for tissue T (H_T) is defined by:

$$H_T = \sum_R W_R D_{T,R}$$

where D_{T,R} is the absorbed dose to tissue T from radiation R, and W_R is the radiation weighting factor. The effective dose E is defined as:

$$E = \sum_T W_T H_T$$

where W_T is the tissue weighting factor. Tables 3 and 4 list W_T and W_R values, respectively. The ICRP recommends that effective doses should not exceed 20 mSv/y for occupational exposure and 1 mSv/y for public exposure [47].

Table 3. Tissue weighting factors W_T (from Ref. [47]).

Tissue	W_T
Bone-marrow (red), colon, lung, stomach, breast, remainder tissues	0.12
Bone surface, brain, salivary glands, skin	0.01
Gonads	0.08
Bladder, oesophagus, liver, thyroid	0.04

Table 4. Radiation weighting factors W_R (from Ref. [47]).

Radiation type (R)	W_R
Photons	1
Electrons and muons	1
Protons and charged pions	2
α particles, fission fragments, heavy ions	20
Neutrons	2.5 + 18.2 exp{−[ln(E_n)]^2/6}, E_n < 1 MeV5.0 + 17.0 exp{−[ln(2E_n)]^2/6}, 1 MeV ≤ E_n ≤ 50 MeV2.5 + 3.25 exp{−[ln(0.04E_n)]^2/6}, E_n > 50 MeV

B. Results

Figure 8 shows the radiation dose received by different organs for a typical human staying on the Martian surface for one year. Figure 8(a) plots the distribution of deposited energy in body organs. The trunk received the highest energy deposition, reaching (9.05 ± 0.04) × 10^{12} MeV/y. The legs received the second highest amount, with (2.02 ± 0.02) × 10^{12} MeV/y per leg, due to their larger mass and volume. The head and skull also showed high deposition, while smaller organs like adrenal glands and thyroid showed the lowest.

Figure 8(b) shows the absorbed dose distribution across body parts, which differs significantly from the energy deposition distribution. The brain received the highest absorbed dose at 62.0$±1.7$mGy/y$, $followedbythyroidandskull.Relativelyhighdoseswerealsoobserved$
$energyparticlesaffectonlysuperficialbodylayers$, $givingupperorganslikebrainandthyroidhigherdosesthanlo$
$bodyabsorbeddosewas$43.8±$0.4 mGy/y.

Accounting for radiation quality, we calculated equivalent doses for different organs (Figure 8(c)). The brain again showed the highest equivalent dose at 234.1$±8.0$mSv/y$, $agreeingwellwithRADdata$[31].$Skull$, $adrenalglands$, $anduperspinealsoshowedhighequiv$
mSv/y. The average whole-body equivalent dose was approximately 153 mSv/y, much lower than RAD data. This difference likely arises because a typical human body is much larger than the RAD detector with non-uniform mass distribution, so lower body parts and internal organs receive less radiation.

To analyze particle contributions, we extracted deposited energy and absorbed dose from electrons, photons, pions, muons, protons, α particles, and heavy ions (Z ≥ 3). Results are plotted in Figure 9 (photon contribution was negligible). Protons deposited (1.08$±0.01)×10^{13}$ MeV/y, accounting for 56.1% of total energy deposition. Electrons contributed 22.6%, while α particles, heavy ions, pions, and muons contributed 6.1%, 3.6%, 6.6%, and 3.9%, re-

spectively. Neutron contribution was only 0.07% due to small reaction cross-sections, with most energy deposited by secondary particles. Particle contributions to absorbed dose were similar, but equivalent dose contributions differed significantly. α particles contributed most to total equivalent dose at 53.7$\pm1.3mSv/y(35.1\pm0.6mSv/y, 32.1\pm$0.7 mSv/y, 20.9%). Electrons, pions, muons, and neutrons contributed only 6.5%, 3.8%, 1.4%, and 0.24%, respectively. Although α particles and heavy ions contributed relatively little deposited energy, they dominated equivalent dose due to their large radiation weighting factors, making them essential considerations for designing radiation protection in future deep-space missions.

As shown in Figures 2–4, simulated spectra for deuterons, tritons, and ^{3}He were much lower than measured data. To assess the impact on dose calculations, we scaled these spectra to match measurements and recalculated doses. The absorbed and equivalent doses for body organs increased by approximately 22% on average, yielding whole-body values of 54.0 mGy/y and 191.6 mSv/y, respectively. This demonstrates that these particles strongly affect dose calculations, and Geant4 models should be improved for better nucleus-nucleus interaction descriptions.

IV. The Shielding Effect of the Martian Soil

The simulation results indicate that doses received by astronauts on the Martian surface are much higher than on Earth, necessitating appropriate radiation protection. For long-term exploration missions, astronauts will likely use Martian soil to build shelters, making the shielding effect of soil worth investigating.

A. Model Setup

A hollow cube (5$\times5\times3m\hat{}\{3\}$) was built in Martian soil with the human phantom placed inside. The soil thickness above the phantom (d) was adjustable. We considered nine thickness levels: d = 0.1, 0.3, 0.5, 0.7, 1.0, 1.5, 2.0, 2.5, and 3 m, computing the dose for each scenario. Primary particles were projected from the soil top according to simulated surface particle spectra.

B. Results

Figure 10 plots radiation doses to the human body at different depths beneath the Martian surface, with surface values included for comparison. Deposited energy, absorbed dose, and equivalent dose all decreased rapidly with increasing soil depth. At depths of 0.1, 0.5, and 1.0 m, absorbed doses were 7.6%, 41.3%, and 71.1% lower than surface values, respectively. The reduction rate decreased as thickness increased further.

Equivalent doses in organs dropped faster than absorbed doses at shallow depths. For example, at 0.1 m depth, equivalent doses to brain and whole body decreased by 30.6% and 28.1%, respectively. This oc-

curs because energetic heavy ions collide with soil and fragment into lighter particles with smaller radiation weighting factors. The variation of effective dose with soil depth was similar to that of dose equivalent. At depths of 0.1, 0.5, and 1.0 m, the effective dose to the whole body was $121.0\$\pm9.7, 67.6\pm7.9, and 35.0\pm2.4 mSv/y, respectively. At 1.5 m depth, the average equivalent and effective doses$ *body effective dose of* $2.7\pm\$1.0$ mSv/y, still above the 1 mSv/y public exposure limit. To confine effective dose below 1 mSv/y, soil thickness must exceed 3 m.

V. Conclusions

This study simulated the Martian surface radiation environment using the Geant4 toolkit. A simple geometrical model and G4QMD physics model were employed. Simulation results for neutrons, photons, protons, α particles, and groups Z = 6–8, Z = 9–13, and Z = 14–24 showed reasonable agreement with RAD data, with average deviations of 60.8%, 56.0%, 27.7%, 37.9%, 40.9%, 60.7%, and 40.1%, respectively. However, for deuterons, tritons, and ^{3}He—pure secondary particles—simulation results were much smaller than RAD data, likely due to underestimated production cross-sections in the G4QMD model.

Particle spectra from the entire upper hemisphere were obtained. Based on the simulated radiation environment, we calculated radiation doses to the human body on Mars. Doses differed significantly between organs. Brain, thyroid, and skull received relatively high absorbed doses, while legs and male genitalia received much lower doses. Average whole-body absorbed and equivalent doses were $43.8\$\pm0.4 mGy/y and 152.9\pm\$2.0$ mSv/y, respectively. Most dose contributions came from α particles, protons, and heavy ions.

The shielding effect of Martian soil was also studied. With increasing soil depth, deposited energy, absorbed dose, and equivalent dose decreased rapidly. At 1.5 m depth, the whole-body effective dose was $17.9\$\pm\$2.4$ mSv/y, below the ICRP occupational exposure limit. However, to achieve the public exposure safe range, soil thickness must exceed 3 m.

Author Contributions: All authors contributed to study conception and design. Material preparation, data collection, and analysis were performed by Jun-Liang Chen, Su-Jun Yun, Tie-Kuang Dong, Zhong-Zhou Ren, and Xiao-Ping Zhang. The first draft was written by Jun-Liang Chen, and all authors commented on previous versions and approved the final manuscript.

Acknowledgments: This work was supported by the National Natural Science Foundation of China (Nos. 12035011, 11535004, 11905103, 11947211, 11975167, 11761161001, 11565010, 11961141003, 11805103, 11673075, 11303107, 11120101005, and 11235001), the National Key R&D Program of China (Nos. 2018YFA0404403 and 2016YFE0129300), the Science and Technology Development Fund of Macau (No. 008/2017/AFJ), the Fundamental Research Funds for the Central Universities (Nos. 22120210138 and 22120200101), and the China Postdoctoral Science Foundation (Nos. 2019M660095 and 2020T130478).

Correspondence: † tkdong@pmo.ac.cn, ‡ zren@tongji.edu.cn

Figures

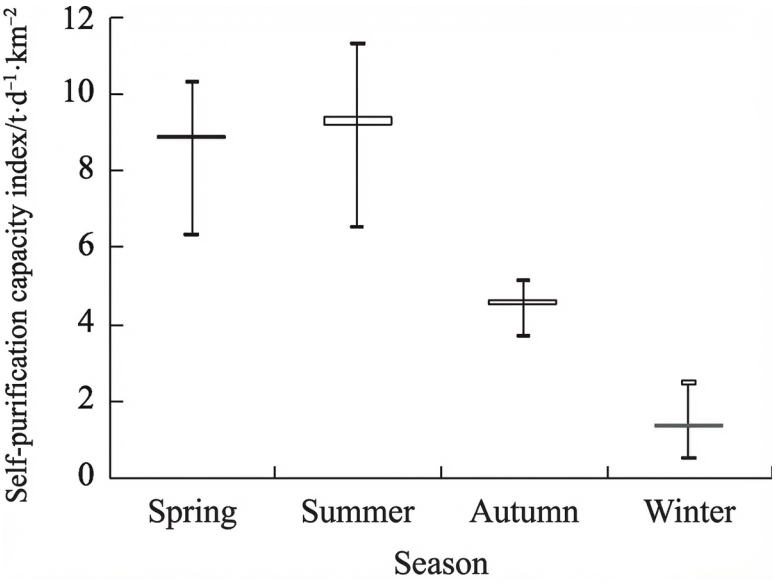

Figure 1: Figure 7

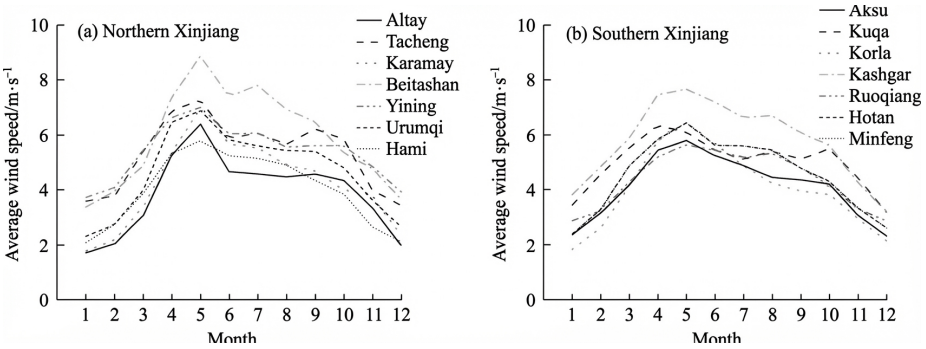

Figure 2: Figure 8

Source: ChinaXiv —Machine translation. Verify with original.